FULL LENGTH PAPER

SECONDARY FLOW IN ROTATING DUCTS

Krishna Sumanth and M. Govardhan
Thermal Turbomachines Laboratory
Department of Mechanical Engineering
Indian Institute of Technology Madras
Chennai-600 036, India
Email : gova@iitm.ac.in

Abstract

A simulation study is performed on laminar flow of an incompressible viscous fluid through rotating ducts. The ducts considered were rectangular straight, rectangular curved and circular curved. Simulations were carried out at two Reynolds numbers, three rotation numbers and five radii of curvature. Secondary flow is induced due to the rotation as well as the curvature of the duct independently, and this can be observed by the presence of double vortex in the bend region and in the downstream region of the rotating duct. Secondary flow creates unwanted losses in the flow. In the present study, the variation of the losses is estimated by plotting the secondary flow kinetic energy and the total pressure loss coefficient for different radii of curvature and rotation speeds. It was observed that both the coefficients increase rapidly in the curved region. The total pressure loss coefficient keeps increasing along the length, while the secondary kinetic energy coefficient decreases after peaking in the curved portion and converges to a constant value. This flow phenomenon, especially in turbines and rotating coolant channels are of practical interest in such applications as heat exchangers, rotors of electrical machinery, cooling channels of gas turbine rotor blades. Therefore it is important to understand the underlying physics, which could help in the design of turbomachines and in optimizing heat transfer rate in the relevant applications.

***Keywords**: Secondary flow, Rotating ducts, Curved ducts, Coriolis force, Centrifugal force, Laminar, Secondary kinetic energy, Total pressure loss coefficient*

Nomenclature

$\bar{C}$ = Bulk mean velocity (m/s)
C_s = Magnitude of secondary flow velocity (m/s)
C_{pt} = Coefficient of total pressure loss
C_{sk} = Coefficient of secondary kinetic energy
D = Cross sectional dimension of the duct (m)
h = Cell size (m)
i, j = Perpendicular directions to the plane of secondary vector
P = Static pressure (Pa)
P_o = Total pressure (Pa)
P_{tref} = Mass averaged total pressure in the reference plane (Pa)
R = Radius of curvature (m)
Ro $= \dfrac{\bar{C}}{2\,\Omega\,D}$
X = Non-dimensional stream-wise distance
Ek = Ekman number $\left(\dfrac{\upsilon}{\Omega\,D^2}\right)$

Greek Symbols

ν = Kinematic viscosity (m^2/s)
ρ = Density of the fluid (kg/m^3)
ω = Vorticity (1/s)
Ω = Angular Speed (rad/s)

Introduction

A three dimensional flow could be categorized into primary flow and secondary flow. Secondary flows are usually in the vicinity of the boundary of the fluid adjacent to solid surfaces where viscous forces are at work, such as

Paper Code : V67 N1/820-2015. Manuscript received on 13 Jun 2013. Reviewed, revised and accepted as a Full Length Contributed Paper on 30 Oct 2014

in the boundary layer. Such a secondary flow occurs when the fluid moves in a curved path. Hence the classic cases would be those of fluid moving in a curved duct or in a rotating duct. Secondary flow in a curved channel acts to replace the slow-moving fluid near the walls with faster-moving fluid, thereby greatly increasing viscous friction at the wall. Frictional losses are increased not only in the bend itself, but also downstream, as a result of the persistence of the secondary flow there. Turbines and compressors have blades which change the direction of the working fluid. There are boundary layers not only on the blades, but also on the hub and casing walls. In general, the fluid in the hub and casing wall boundary layers is turned more than the fluid outside the boundary layers, and impinges on the next set of blades at an increased angle of incidence.

Materials as well as momentum may be transported by secondary flow. Heat transfer and momentum transfer follow similar laws, so that changes in the flow distribution which promote heat transfer generally cause increased friction, and vice versa. Heat exchangers are sometimes made with wavy passages, to promote secondary flow. The resultant heat transfer (and friction) can be more than double that of a comparable straight passage.

Benton [1] used a perturbation expansion and showed that for laminar flow in circular pipes secondary flow consisted of double-vortex configuration. Subsequent to this study, Benton and Boyer [2] examined the case of laminar flow in a rapidly rotating duct of arbitrary cross-section. When the Reynolds number is not too large and when the ratio (ε) of Rossby number to Reynolds number is small (i.e. $<< 1$), it was shown that the viscous effects are significant only in the thin boundary layer near the walls of the duct and also that the inertia effects were negligible everywhere. For laminar flow in a rotating rectangular channel, Hart [3] conducted experimental as well as a theoretical study. He observed the presence of a weak double vortex in the channel at low rates of rotation. Wagner and Velkoff [4] also observed double vortex for a turbulent flow through the rotating rectangular duct. In his numerical study of laminar, incompressible and viscous flow through rotating rectangular ducts, Speziale [5] conducted the studies for moderate to relatively high rates of rotation. He showed that for weak rotation rates, the double vortex formed in the cross section is independent of the aspect ratio of the rectangular cross section. At the low Reynolds number, numerical analysis in straight and curved square ducts by Baek and Ko [6] also showed double vortex formed in cross section and the center of the vortex moves closer to the upper boundary with increase in the rotation speed. This is because of the increasing effect of the secondary flow with rotation speeds (expressed as reduction in the Ekman number).

A few years later, Lezius and Johnston [7] found that the critical disturbance mode for laminar flow occurred at a Reynolds number of 88.53 and a rotation number of 0.5. Thangam and Hur [8] studied the secondary flow of an incompressible viscous fluid in a curved duct by using a finite-volume method. They showed that as the Dean number increases, the secondary flow structure evolves into a double vortex pair for low-aspect-ratio ducts and roll cells for ducts of high aspect ratio. They found that for ducts of high curvature the onset of transition from single vortex pair to double vortex pair or roll cells depends on the Dean number and the curvature ratio, while for ducts of small curvature the onset can be characterized by the Dean number alone. They developed a correlation for the friction factor as a function of the Dean number and aspect ratio and it was in good agreement with the then available experimental and computational results for a wide range of parameters.

Flow visualization studies were made by Cheng and Wang [9] for rotating radial straight pipes for higher Reynolds numbers and rotation speeds and captured the transition to turbulence and the re-laminarization phenomenon. Hoshio Tsujita [10] examined the effects of passage vortex in a turbulent flow in curved rectangular ducts using computational methods. They inferred that the passage vortex contributed predominantly to the generation of losses not only in the breakdown process but also in the development process. Qin and Pletcher [11] studied the velocity field and instability of the flow in a rotating square duct. They compared their theory with the experimental results of Smirnov and Yurkin [12]. The critical rotation numbers obtained were in qualitative agreement with experimental data.

Most of the previous investigations, of either laminar or turbulent flow regime, which have been done on curved ducts or straight ducts, involved developing relations among the flow conditions, velocity profiles and vortex formations. However, the mechanism of loss generation in curved ducts has not been fully clarified yet. Investigations have been made on generation of losses due to passage vortex or secondary flow in to a turbulent flow through rectangular ducts. But these studies were done for a constant radius of curvature, single cross section and turbulent regime. Hence, this study is an attempt to investigate the effect of curvature and cross sectional shape on the loss generation due to secondary flows in rotating ducts.

Computational Model

The case to be considered first is that of a laminar flow of an incompressible viscous fluid in a straight square duct. The duct is rotated with an angular velocity of Ω about an axis perpendicular to the axis of the duct. In the model created, axis of duct is parallel to the x-axis and the rotation is about the global z axis.

All the simulations in the project were done using various tools of ANSYS 13.0. The computational domain is modeled in ICEM CFD.

Geometry - Straight Square Duct

The 3D models of the ducts were created using the 'Design Modeler' tool in ANSYS 13.0. The straight duct is of length 40D, D being the dimension of the cross section. D is chosen as 0.03m. The cross section is sketched on the YZ plane and then extruded in X-direction to a length of 40D. The axial direction of the duct is parallel to x axis while the duct is rotated about z axis, (Fig.1(a)).

The mesh of the duct is generated using ICEM CFD. A block was created for the entire model and all the edges were associated to corresponding edges of the model. All the four edges of the cross section are divided into 30 nodes, with a starting spacing of 0.0002 m near the walls, with a growth ratio of 1.2 using 'BiGeometric' mesh law in the pre mesh parameters. A total of 200 nodes of 'uniform' mesh law are created along the length of the duct. A hexagonal mesh is created for the model.

Geometry - Curved Square Duct

The entrance length and the exit length for curved duct are kept constant at 45 D and 30 D, D being the dimension of cross section. D here is chosen to be 0.03 m. The axis of rotation is the global x-axis, which is parallel to the axial direction of the entrance section of the duct, (Fig. 1(b)). Fig.1(a) shows the orientation of axes for the straight duct. This duct which is used for validation rotates about z-axis. The 3D models were created using the Design Modeler of ANSYS 13.0.

The meshing was generated using ICEM CFD. First, a block is created for the entire model and it was split into three blocks. The edges associated to each block were associated to the edges of the parts in each zone i.e. entry, curved and exit zones. For the cases where in the radius of curvature is large, i.e. 5 D and 10 D, the curved region block was further split into 3 blocks. The mesh configuration in the cross section is same as that of a straight duct. 30 nodes on all the edges with a BiGeometric mesh law. Along the length of the duct, a total of 100 nodes in the entry section, 10 nodes per block in the curved section, and 75 nodes in the exit section were created with uniform mesh law. Since the number of blocks in the curved region varies with radius of curvature, the total number of nodes and elements vary for each of the curved ducts. Fig.2 shows a side view of the curved duct with measuring planes. Fig.3(a) is a close view of the mesh generated in the curved region.

To estimate the discretization error, Grid Convergence Index (GCI) study based on the Richardson Extrapolation (RE) method was performed. The three grids used with the GCI method are 107712 (coarse), 207727 (medium) and 350697 (fine). The grid size $h_1 < h_2 < h_3$ was maintained. These three different sets of grid are geometrically similar, each with a grid refinement factor (r) greater than 1.3. Procedure for calculating GCI and discretization error is adopted from Roache et al.[13].

Table-1 presents the calculation of discretization error for total pressure at the exit of the rotating curved duct at Re = 500. The value of GCI is below 1%, which indicates an accurate calculation. Fig.3(b) shows the value of total pressure variation at the exit of the duct with number of elements. The value with fine grid matches with the extrapolated value.

For straight duct, number of nodes and number of elements are 180000 and 192125 respectively. The number of elements for the curved duct is 350697. The numbers are arrived at after conducting grid independence study. Grid independence study was conducted as per the procedure given by Roache et al.[13].

Fluid Model

The fluid selected for the simulations was air at 25°C, with a reference pressure of 101325 Pa. The domain was set to rotating mode, with the axis specified as described in the previous sections. Simulation type was set as steady

Table-1 : Grid Independence Study

No. of Elements N1, N2, N3	350697, 207727, 107712
r_{21} (h_2/h_1)	1.2
r_{32} (h_3/h_2)	1.25
Total Pressure at the outlet (fine grid)	182.908 Pa
Total Pressure at the outlet (medium grid)	184.436 Pa
Total Pressure at the outlet (fine grid)	184.732 Pa
Extrapolated value	182.7 Pa
Approximate relative error	-0.84%
Extrapolated relative error	-0.1%
CGI fine grid	-0.12%

state. The boundary conditions considered for various cases are given as follows:

For Re = 10 and 500, the flow velocity at inlet is given as 0.0053 and 0.265 m/s respectively. The outlet static pressure is given as 0 Pa relative to atmospheric pressure. The walls are given no slip condition.

Results and Discussion

The results from the simulations of all the cases are presented in this section. The case of no rotation for the straight duct gives a basic understanding of how the secondary flow affects the flow in the presence of a non-zero rotation or a curve in the duct, followed by the results for the rotating curved ducts. The losses arising due to secondary flows are measured using Total Pressure Loss Coefficient (C_{pt}) and Coefficient of Secondary Kinetic Energy (C_{sk}), which are defined as follows (Hoshio Tsujita [10]):

$$C_{pt} = \frac{P_{tref} - P_o}{0.5\, \rho\, \bar{C}^2} \tag{1}$$

$$C_{sk} = \left(\frac{C_s}{\bar{C}}\right)^2 \tag{2}$$

Where P_{tref} is the mass averaged total pressure near the reference plane (i.e. x = 0, here the plane at 0° of the bend) and P_o is the total pressure at a point. C_s is the secondary velocity defined as

$$C_s = \sqrt{\upsilon_i^2 + \upsilon_j^2} \tag{3}$$

where i and j are the perpendicular directions in the plane of the secondary vector i.e. (y, z) for entry section, (y, x sin θ - z cos θ) for the planes in the curved section (θ is the angle between the plane's normal and x-axis) and (x, y) in the exit section. $\bar{C}$ is the bulk mean velocity of the fluid.

Stationary Case

In the case of a straight square duct, in the absence of rotation, there is no secondary flow taking place because there is neither centrifugal force nor the Coriolis force. Hence the case reduces to an incompressible, viscous flow through a square channel and the fluid attains a quasi-parabolic profile inside the channel after the flow is fully developed. The Figs.4 and 5 illustrate the same.

Validation of Straight Square Duct

The results from the case of rotating straight square duct were compared to those of Baek and Ko [6] and the results showed a good agreement. The results and comparison are showed in detail in this section.

Cases Considered :

Re = 10	Ek = 0.1, 0.01, 0.001	Ro = 0.00507, 0.0507, 0.507
Re = 500	Ek = 0.1, 0.01, 0.001	Ro = 0.253, 2.53, 25.3

Where Ek is Ekman number $\left(\mathrm{Ek} = \frac{\nu}{\Omega\, D^2}\right)$ and Ro is Rossby Number $\left(\mathrm{Ro} = \frac{\bar{C}}{2\,\Omega\, D}\right)$.

Coriolis forces play dominant role in curved rotating ducts, Ekman number, Ek (ratio of viscous forces to Coriolis forces) is used in the present analysis. Rossby number, Ro (ratio of interial forces to Coriolis forces) will be in fixed proportion to Ekman number for a given Reynolds number and fluid viscosity. In the present investigations the ratio of Ro/Ek ≈ 253. The value of Rossby number is also mentioned in the text.

Figures 6 and 7 show the comparison of axial velocity (non-dimensional) along the vertical center plane from simulation with that of Baek and Ko [6]. The agreement between the results is quite good. The axial velocity profile distorts from a quasi-parabolic profile (when $\Omega = 0$, as shown in Figs.4 - 5) to a flatter profile as the speed of rotation increases (i.e. as Ekman number decreases). This can be observed from Figs.6 and 7. This means that the axial velocity gradient along the center plane is reduced, and hence its maximum value is also reduced. This is the effect in the vertical plane.

Convective inertia term is weak at low Reynolds number (Re = 10). The center of vortex moves to upper and lower wall, as the rate of rotation increases, (Fig.6). Because the rate of rotation is small at high Ekman number (Ek = 0.1), Coriolis force does not have a substantial effect on the flow. Therefore the axial velocity profile shown in Fig.6 has quasi-parabolic velocity distribution. But at low Ekman number (Ek = 0.001), the Coriolis force dominates flow in the duct interior except in the region of thin viscous boundary layers.

At high Ekman number (low rotational speed), the secondary flow is weak but at low Ekman number (high rotational speed), the magnitude of the secondary flow is comparable to axial velocity. As the speed of rotation increases, the strength of the secondary flow becomes larger. At low Ekman number (Ek = 0.001) the maxima in the axial velocity are closer to the end walls and the flow has nearly uniform axial velocity profile in the vertical planes of the duct as can be seen in Fig.6. The axial velocity along the vertical centreline of the duct is symmetric and begins to flatten in the core region of the duct with the increase of rotation rate. When Ekman number is 0.001, the gradient of the axial velocity along the vertical centreline is zero in the core region and the peaks of the axial velocity are closer to the walls.

When inertia plays a significant role (Re = 500), more complicated flow evolves. Figs.7 - 9 show the variation of axial velocity for different Ekman numbers in vertical plane. When Ekman number is high (Ek = 0.1), a double vortex secondary flow appears in the transverse planes of the duct, (Figs.7, 8(a), 9(a)). But as the speed of rotation increases, the secondary flow with two vortices is split into a four-vortex secondary flow, (Figs.8(b) and 9(b)). If the rotation rate is increased further, the secondary flow restabilizes to a slightly asymmetric double-vortex configuration, (Figs.7, 8(c), 9(c)). The unstable flow with a four-vortex results from a disparity in the symmetry of the convective and the Coriolis terms. But the unstable flow with a four-vortex (Ek = 0.01) shows three peaks in velocity profile, (Fig.7). As the rate of rotation increases further, the axial velocity profile on the vertical centre plane shows two peaks in the near region of the upper and lower walls with the plateau in core region. The secondary flow distorts substantially the axial velocity profile even though the magnitude of secondary flow is small, that is, Coriolis force has a substantial effect on the axial velocity flow profile.

Rotating Curved Ducts

In the present study so far, the primary reason for inducing secondary flows has been Coriolis force (rotating straight ducts). But, in the case of curved ducts, two forces induce the secondary flows in the rotating duct - Centrifugal force and Coriolis force. Both the forces do so individually. Centrifugal force is responsible for the secondary flow created in the bend region of the duct, while the Coriolis force is responsible for the secondary flow in the downstream region from the curve. The effects of these two forces are distinguishable from axial velocity contour diagrams and secondary flow vector diagrams.

Figure 10 shows axial velocity contours from various sections of the curved duct as marked in Fig.2. In Fig.10(a) - 10(c), the shift of the velocity contours towards the right side could be observed. Right side here signifies the radially outward direction which is caused due to the centrifugal force. With the secondary flow effects coming in, the velocity profile becomes flatter with its gradient in the vertical direction close to zero. This can be observed in Fig.10(d). The fluid is then significantly far away from the axis of rotation to experience the Coriolis force. This, along with the diminishing centrifugal force (as the fluid surpasses the curved region) allows Coriolis effects to dominate and hence the bulk of the fluid velocity slowly moves to the trailing edge of the rotating duct (Here to the top edge of the cross section). This can be observed in Figs. 10(e) - 10(h).

In the following figure (Fig.11), the same effects are shown through the secondary flow vectors. Fig.11(a) shows the secondary flow vectors at section ‘c’ in Fig.2 and Fig.11(b) shows secondary flow vectors at section ‘i’ in Fig.2. Both are drawn to the same scale. Here in Fig.11(a), the double vortex is symmetrical about the horizontal center plane while in Fig.11(b), the double vortex is symmetrical about the vertical center plane. This shift starts at about the end of curved region and takes place through the downstream region in the exit section. Another important thing to notice here is the magnitude of the vectors. The magnitude in Fig.11(a) is about 0.13 m/s while in that of in Fig.11(b) is an order less, around 0.01 m/s (The common legend for both the figures is shown in Fig.11(c)).

Secondary flows create unwanted losses in the flow. These losses can be quantified using Total Pressure Loss Coefficient and the Secondary Kinetic Energy Coefficient as defined in equations (1) and (2). In this section, a stream-wise variation of these losses with stream wise distance X (non-dimensional) is shown for various radii of curvature, Ekman numbers and different cross sections.

Variation of Losses with Ekman Number

This section presents the variation of both the coefficients with Ekman number for all the cases. Stream wise distance X (non-dimensional) is defined as l/D, where l is the stream wise distance from the reference plane and D is the cross sectional dimension. The area of interest is to the right of the origin. The following Figs.12, 13, 14, and 15 show the variation of total pressure loss coefficient for radii of curvature 1D, 2.5D, 5D and 10D of curved square duct respectively. In all the four figures, it is seen that the losses increase with the Ekman number.

Variation of Losses with Radius of Curvature

The following (Figs.16 - 18) show the stream-wise variation of total pressure loss coefficient for different radii of curvature at all the Ekman numbers. The loss coefficient decreases with increase in the radius of curvature. In all the figures, duct with 1D curvature has the highest pressure loss, while the one with 10D curvature has the least pressure loss coefficient. It is also observed that as the speed of rotation increases, the slope of the lines in the exit section increases, and can be clearly seen in the case of 5D and 10D lines. In fact, in Figs.17 and 18, 5D and 10D lines have smaller slopes in the curved section than in the exit section.

The stream-wise variation of coefficient of secondary kinetic energy with respect to radius of curvature is shown in Figs.19-21. The coefficient of secondary kinetic energy decreases with increase in radius of curvature. It is highest for the duct with curvature 1D and least for the duct with curvature 10D. The difference in peaks reduces with increase in rotation speed. An important observation is that all the lines are converging to about the same value in the exit section of the duct. This proves the dominance of curvature over rotation in contributing to the losses.

Variation of Losses with Shape of the Cross Section

The value of the coefficient also depends on whether the cross section is square or circular. Since we have chosen area as the constant parameter, the value of hydraulic diameter is different for both. D is 0.03 m for the square while it is 0.0339 for the circle. Hence the amount of wetting surface is less for circular duct compared to a square duct and consequently the frictional losses in the circular duct would be less. This is reflected is Fig.22 which compares C_{pt} of square duct and circular duct for same conditions. Important observation here would be the lower slope of the circular duct lines.

The following figure compares the secondary kinetic energy of both the ducts under similar conditions. Since the diameter of the circle is more than the side of the square, for the same Ekman number, the circular duct rotates with a slightly slower speed of rotation and hence experiences lesser secondary kinetic energies in the flow. This is shown in Fig.23.

Conclusions

Secondary flow analysis was performed on rotating ducts for various cases. After analyzing the results, the major conclusions drawn from the present study are as follows:

- In the case of straight duct, Coriolis force induces the secondary flow. Flow destabilizes due to rotation by forming a pair of double vortices. The flow re-stabilizes at higher rates of rotation and the axial velocity attains a uniform profile in the duct.
- In the case of curved ducts, secondary flow effects appear individually, due to both centrifugal force (in the bend region) and Coriolis force (in the exit region).
- Centrifugal forces dominate in the curved region compared to the Coriolis force. Hence the secondary flow effects in the curved region are mainly due to the centrifugal force.
- The total pressure loss coefficient increases with increase in the rotational speed and decreases with an increase in the radius of curvature. This is because of

the inverse relation between the radius of curvature and the centrifugal force.

- For ducts with lower radius of curvature (1 D and 2.5 D), the total pressure loss coefficient increases more rapidly in the curved region of the duct compared to the exit region while for ducts with higher radius of curvature, it increases less rapidly in curved region compared to that in the exit region.
- The coefficient of secondary kinetic energy increases with an increase in the rotation speed and decreases with an increase in the radius of curvature. The value of the coefficient peaks in the curved region for any curvature at any speed. Hence the intensity of losses due to centrifugal forces is more than that of Coriolis force.
- The coefficient of secondary kinetic energy converges to about the same value for different radii of curvature at all the Ekman numbers. This shows the independence of the losses created due to the secondary flows in the exit section.
- The difference among the peak values of coefficients of secondary kinetic energy for different radii of curvature decreases with increase in the speed of rotation. This coupled with the fact that its value increases with the speed of rotation shows strong dependence of secondary flow effects due to centrifugal forces on speed of rotation.
- The coefficient of total pressure loss varies more rapidly for a square curved duct compared to a circular curved duct. The coefficient of secondary kinetic energy has lesser values for a circular duct compared to a square duct for the same Ekman number and radius of curvature.

References

1. Benton, G.S., "The Effect of the Earth's Rotation on Laminar Flow in Pipes", Journal of Applied Mechanics, Vol.23, pp.123-127, 1956.
2. Benton, G. S and Boyer, D., "Flow Through a Rapidly Rotating Conduit of Arbitrary Cross Section", Journal of Fluid Mechanics, Vol. 26, pp. 69-79, 1966.
3. Hart, J.E., "Instability and Secondary Motion in a Rotating Channel Flow", Journal of Fluid Mechanics, Vol.45, pp. 341-351, 1971.
4. Wagner, R.E and Velkoff, H.R., "Measurements of Secondary Flows in a Rotating Duct", Journal of Engineering for Power, Vol. 94, pp.261-270, 1972.
5. Speziale, C.G., "Numerical Study of Viscous Flow in Rotating Rectangular Ducts", Journal of Fluid Mechanics, Vol.122, pp.251-271, 1982.
6. Baek, J.H and Ko, C.H., "Numerical Flow Analysis in a Rotating Square Duct and a Rotating Curved-Duct", International Journal of Rotating Machinery, Vol.6, No.1, pp.1-9, 2000.
7. Lezius, D.K and Johnston, J.P., "Roll-cell Instabilities in Rotating Laminar and Turbulent Channel Flows", Journal of Fluid Mechanics, Vol.77, pp.153-175, 1976.
8. Thangam, S and Hur, N., "Laminar Secondary Flow in Rectangular Ducts", Journal of Fluid Mechanics, Vol.217, pp.421- 440, 1990.
9. Cheng, K.C and Wang, L., "Secondary Flow Phenomenon in Rotating Radial Straight Pipes", International Journal of Rotating Machinery, Vol.2, No.2, pp.103-111, 1995.
10. Hoshio Tsujita., "Numerical Investigation of Loss Generation Mechanisms of Flow in Turbomachinery by Using Curved Square Duct", Journal of Thermal Science, Vol.2, No.3, pp.219-224, 2003.
11. Qin, Z and Pletcher, R.H., "The Velocity Field and Instability of Rotating Duct Flow", Journal of Physics of Fluids, Vol.104-106, pp.1-18, 2007.
12. Smirnov, E.M and Yurkin, S.V., "Fluid in a Rotating Channel of Square Section", Journal of Fluid Mechanics, Vol.6, pp.24, 1983.
13. Roache, P. J., Ghia, K. N and White, F. M., "Editorial Policy Statement on the Control of Numerical Accuracy", ASME Journal of Fluids Engineering, Vol.108, No.1, pp.1-7, 1986.

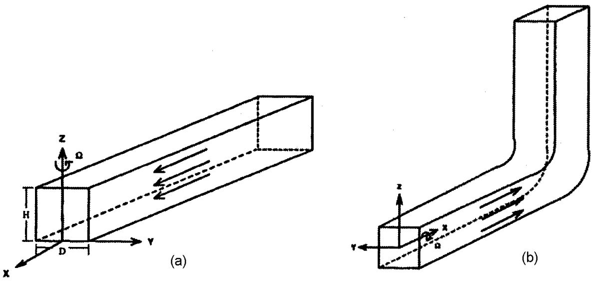

Fig.1 Orientation of the Axes and the Flow Direction (a) Straight Duct (b) Curved Duct

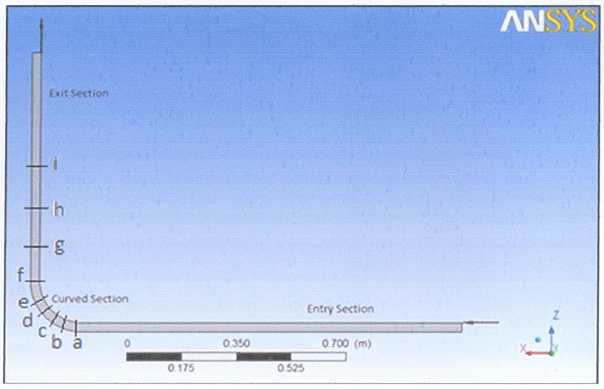

Fig.2 A Side View of a Curved Duct Model with Measuring Planes

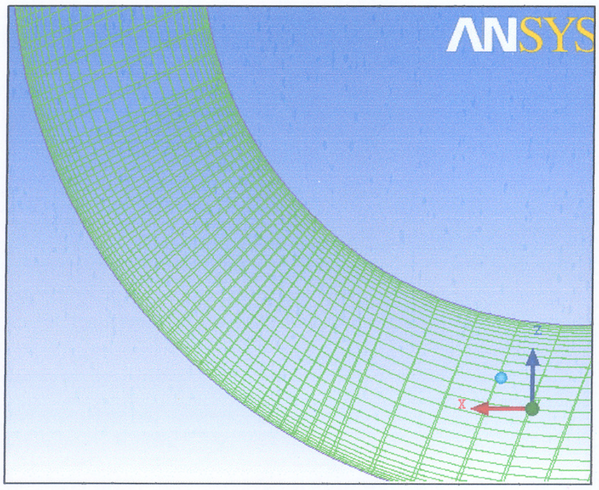

Fig.3(a) A Closer View of the Mesh Generated in the Curved Region

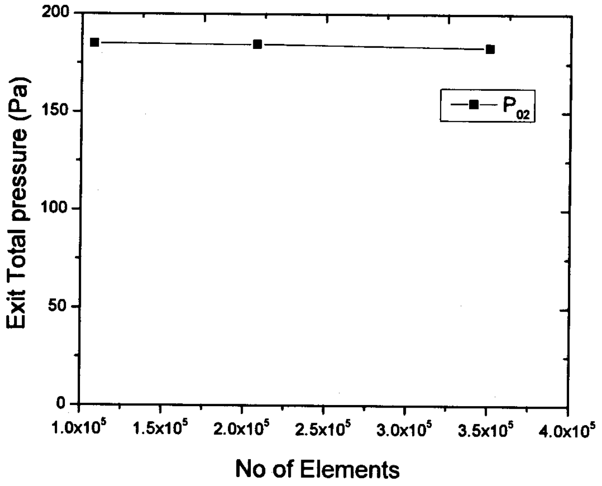

Fig.3(b) Variation of Total Pressure at the Exit of the Rotating Duct with Number of Elements (Re = 500)

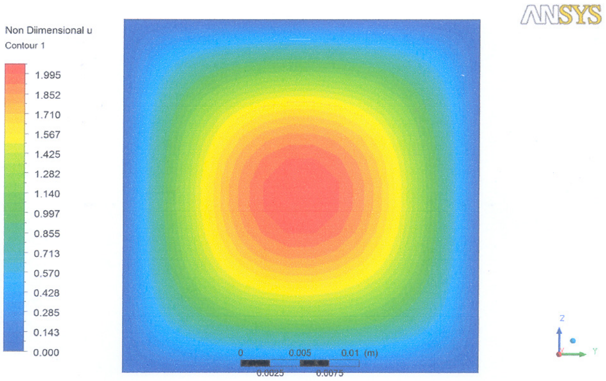

Fig.4 Axial Velocity Contours of a Stationery Straight Duct

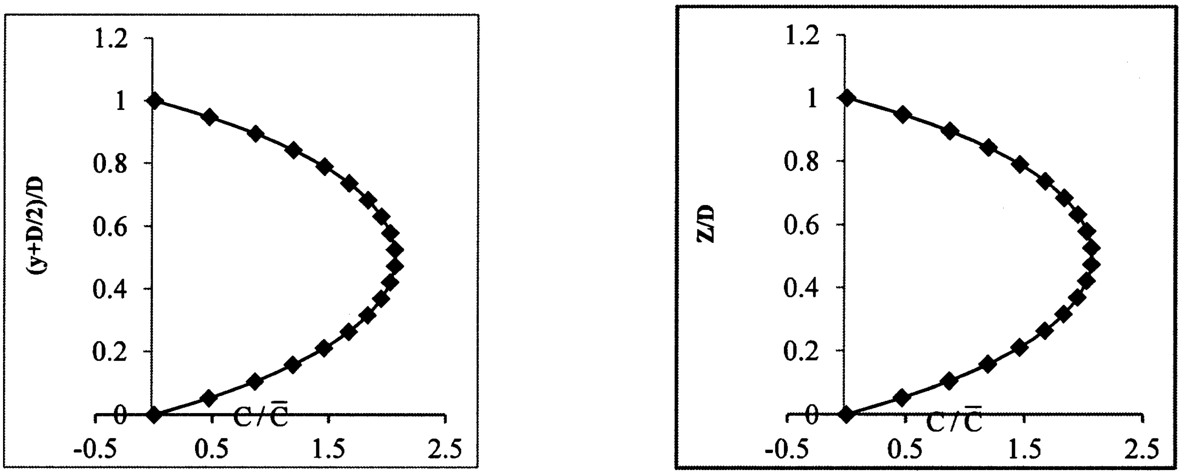

(a) (b)

Fig.5 Variation of Axial Velocity in (a) Horizontal and (b) Vertical Center Planes

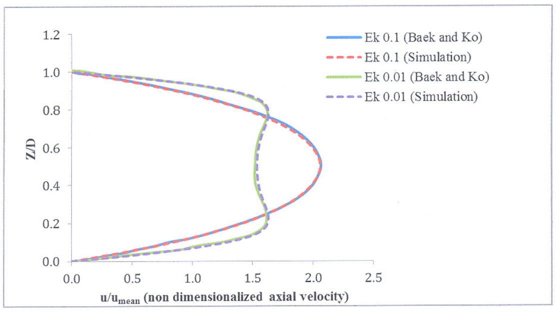

Fig.6 Variation of Axial Velocity in the Vertical Center Plane for Re = 10 in Straight Duct

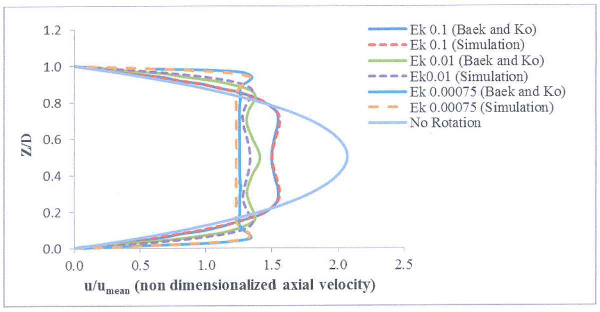

Fig.7 Variation of Axial Velocity in the Vertical Center Plane for Re = 500 in Straight Duct

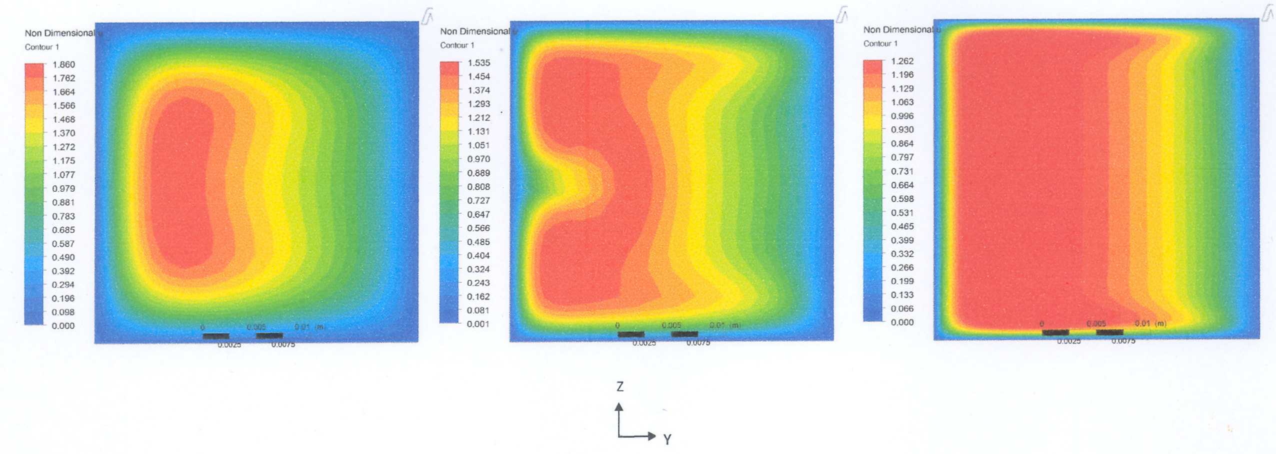

(a) Ek = 0.1 , Ro = 25.3 (b) Ek = 0.01, Ro = 2.52 (c) Ek = 0.001, Ro = 0.253

Fig.8 Axial Velocity Contours in the Cross Section of the Straight Duct

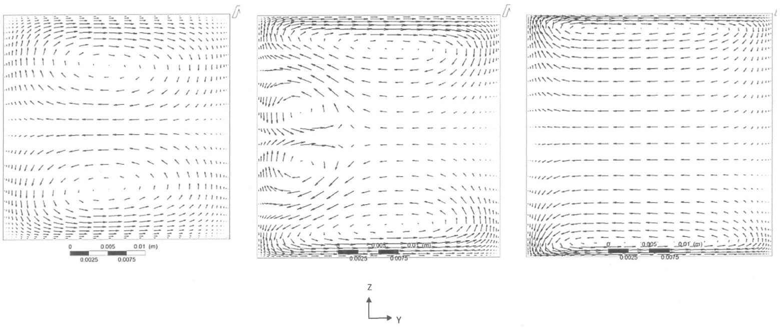

(a) Ek = 0.1, Ro = 25.3 (b) Ek = 0.01, Ro= 2.53 (c) Ek = 0.001, Ro = 0.253

Fig.9 Secondary Flow Vectors in the Cross Section of the Straight Duct

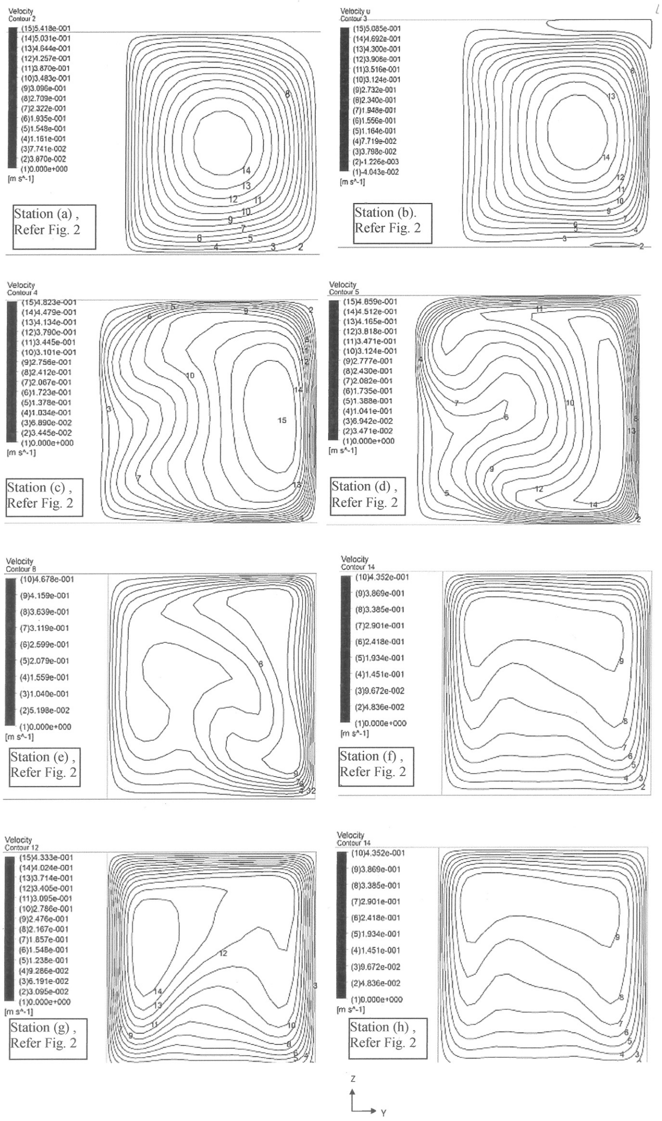

Fig.10 Avial Velocity Contours at Various Sections of Duct

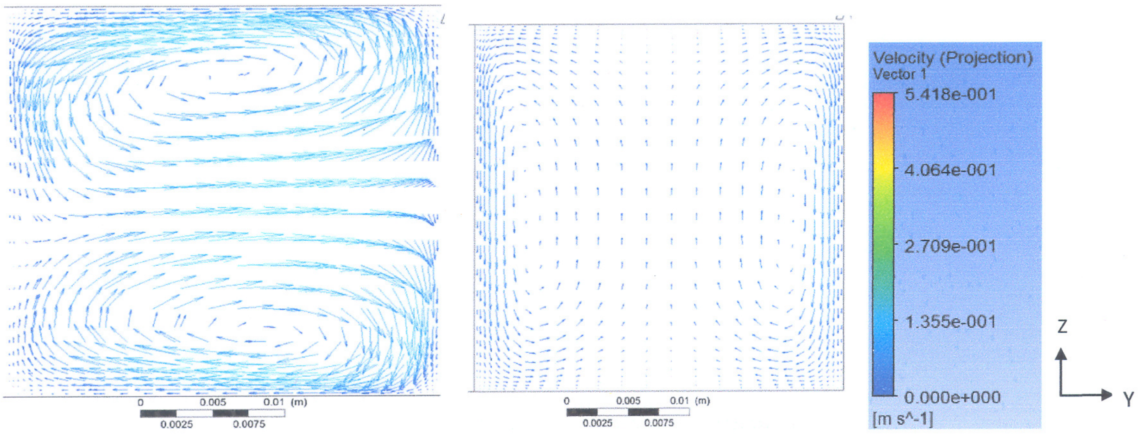

(a) (b)

Fig.11 Secondary Flow Vectors in the Cross Sections of the Curved Duct (a and b are at sections 'c' and 'i' in Fig.2)

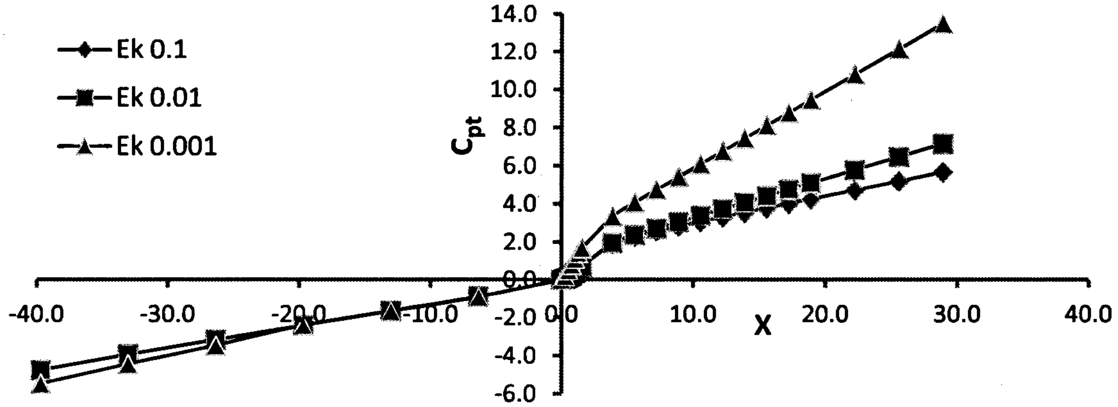

Fig.12 C_{pt} vs X for R = 1D, Curved Square Duct

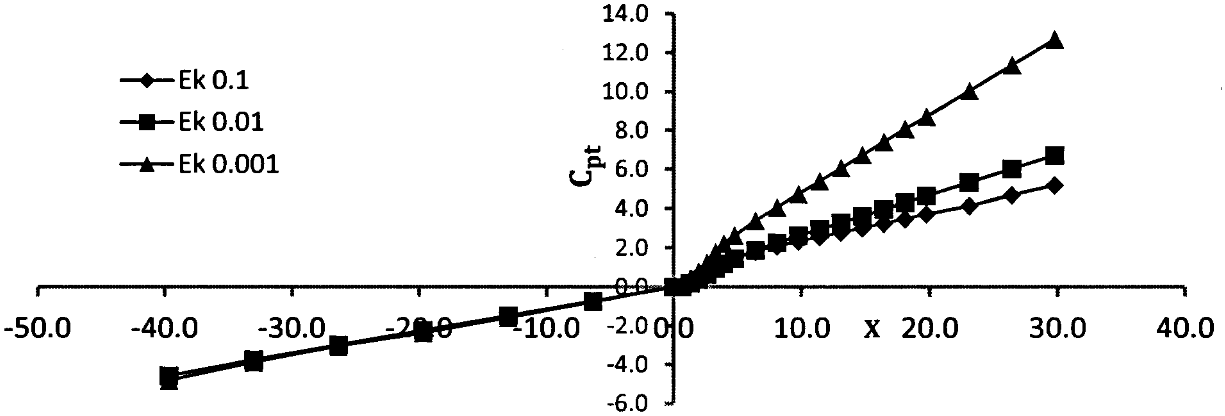

Fig.13 C_{pt} vs X for R = 2.5D, Curved Square Duct

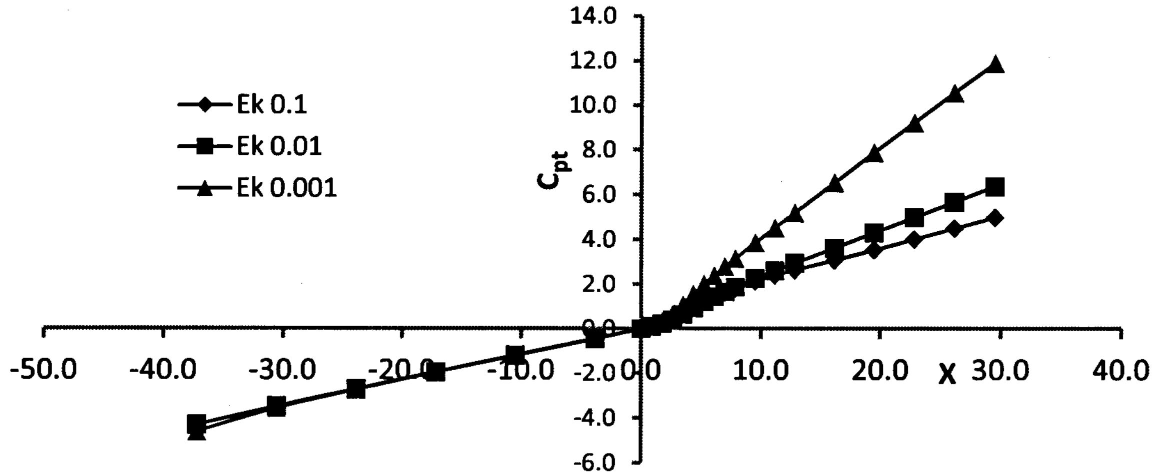

Fig.14 C_{pt} vs X for R = 5D, Curved Square Duct

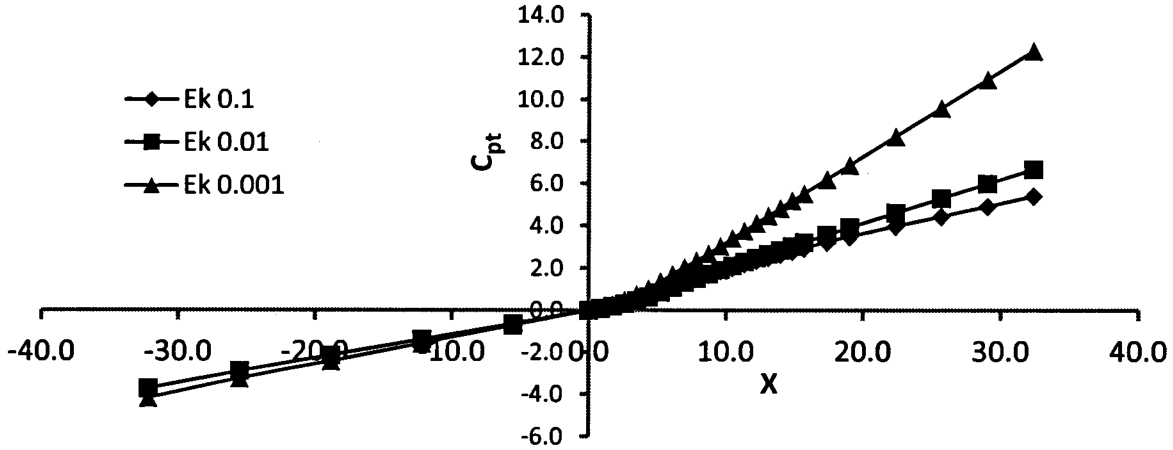

Fig.15 C_{pt} vs X for R = 10D, Curved Square Duct

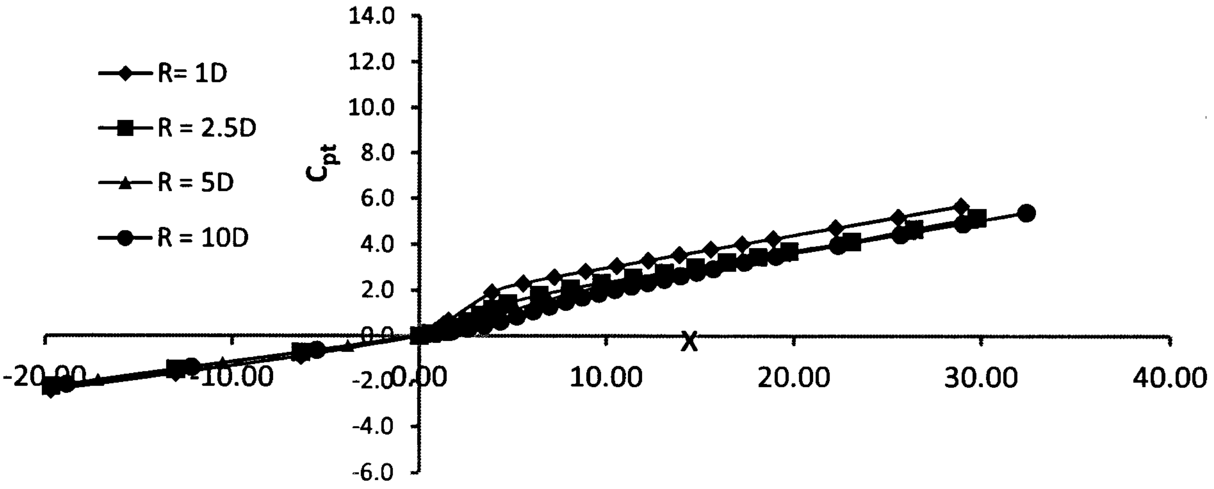

Fig.16 Stream-wise Variation of C_{pt} at Ek = 0.1 for Various Radii of Curvature

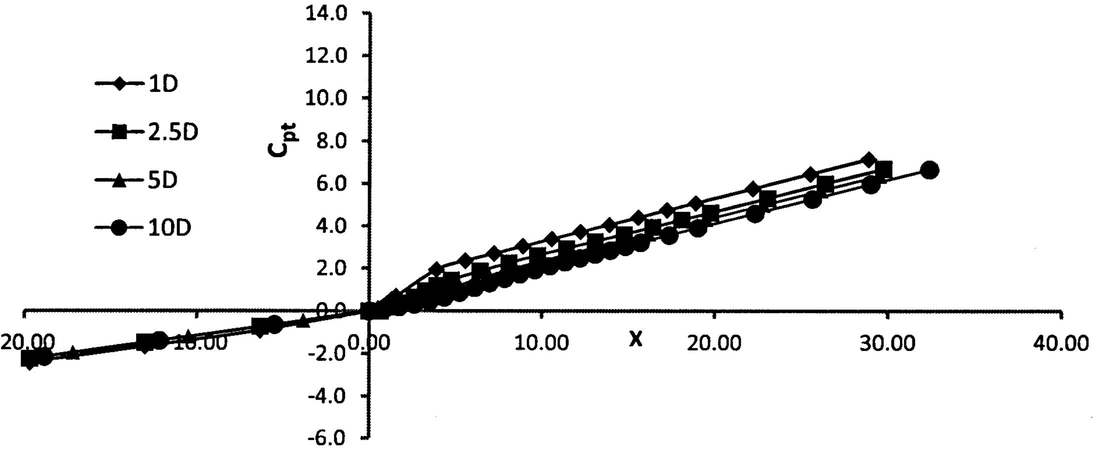

Fig.17 Stream-wise Variation of C_{pt} at Ek = 0.01 for Various Radii of Curvature

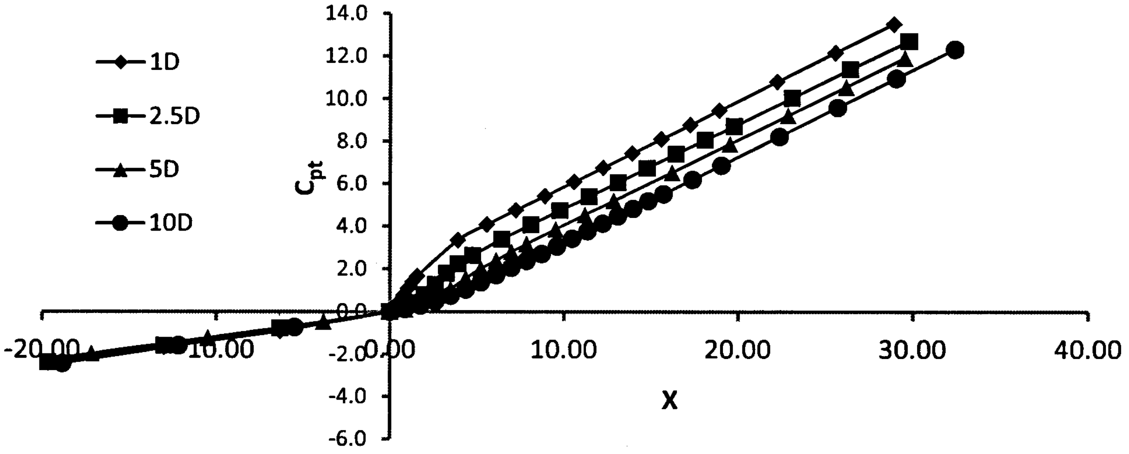

Fig.18 Stream-wise Variation of C_{pt} at Ek = 0.001 for Various Radii of Curvature

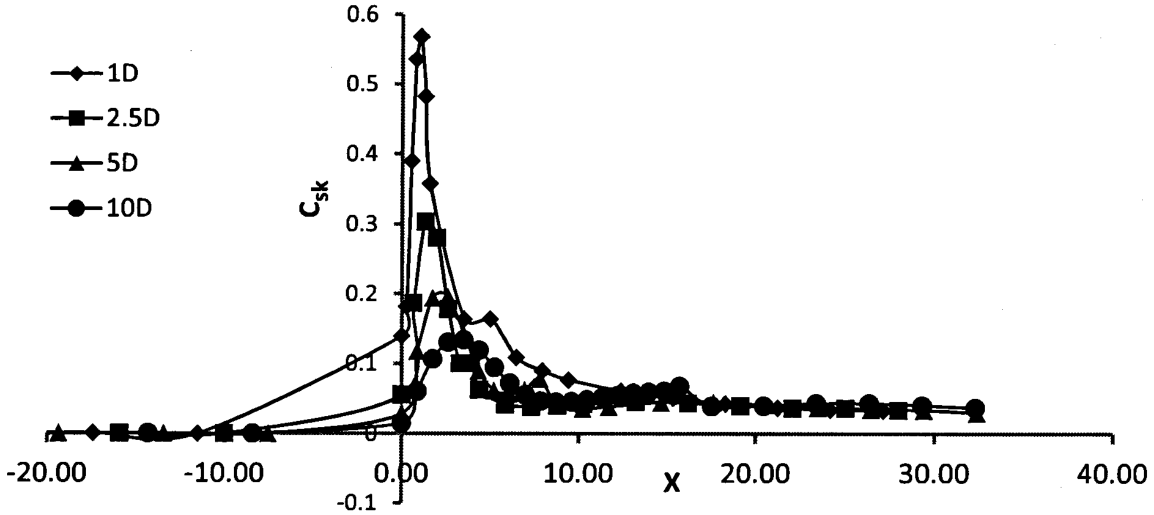

Fig.19 Stream-wise Variation of C_{sk} at Ek = 0.1 for Various Radii of Curvature

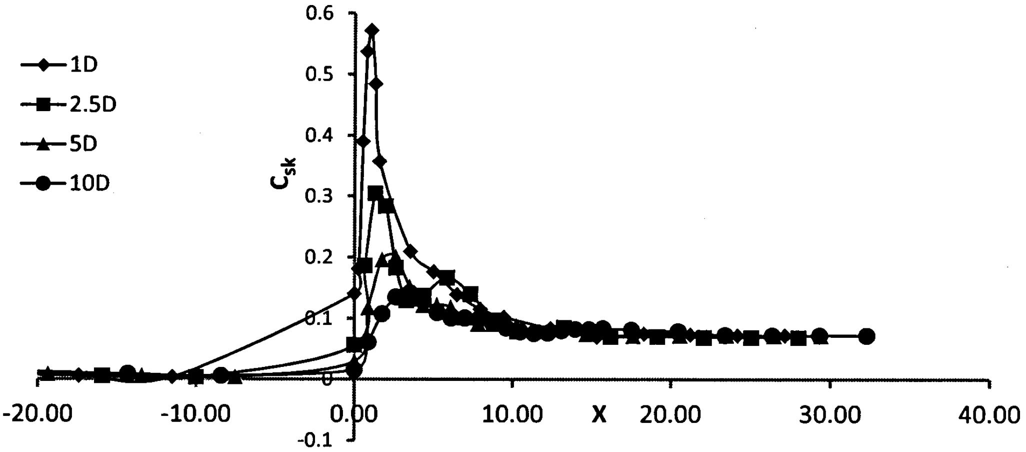

Fig.20 Stream-wise Variation of C_{sk} at Ek = 0.01 for Various Radii of Curvature

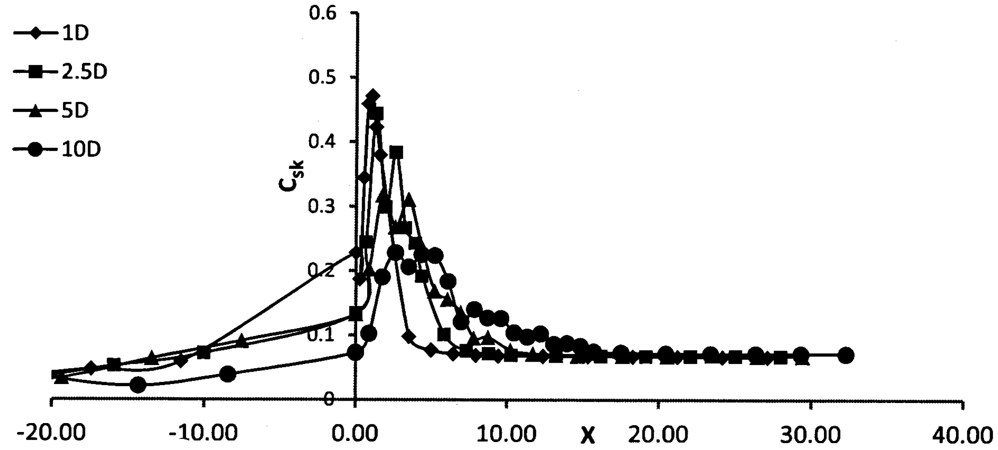

Fig.21 Stream-wise Variation of C_{sk} at Ek = 0.001 for Various Radii of Curvature

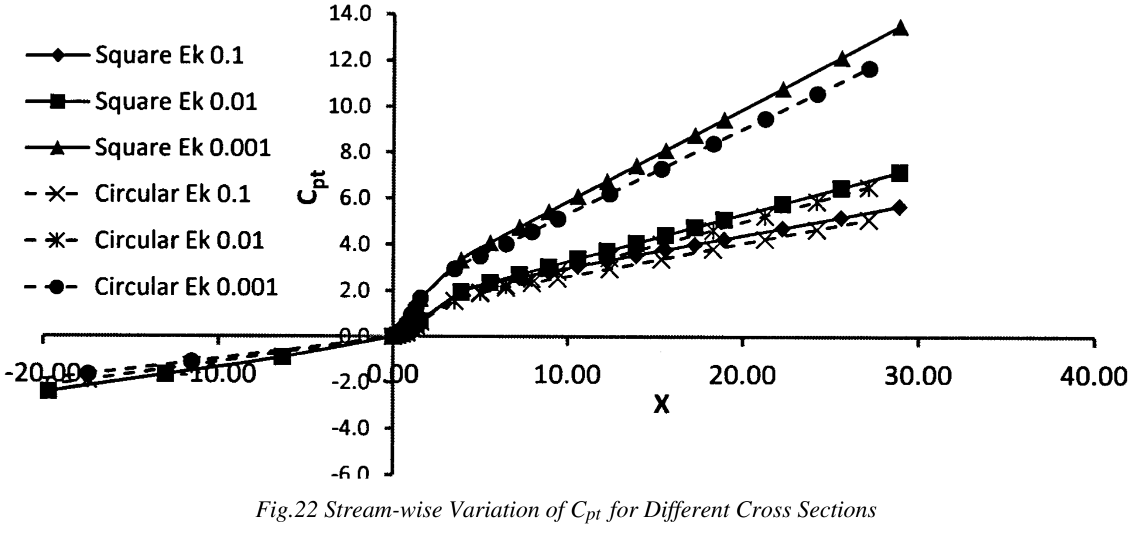

Fig.22 Stream-wise Variation of C_{pt} for Different Cross Sections

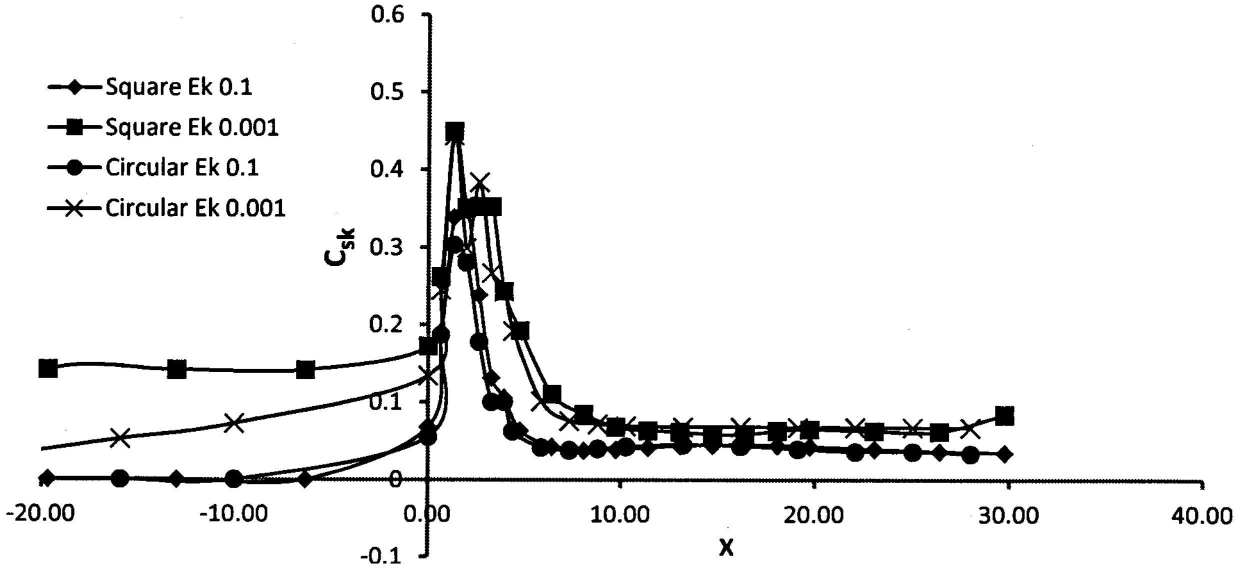

Fig.23 Stream-wise Variation of C_{sk} for Different Cross Sections